Low Temperature Physics/Fizika Nizkikh Temperatur, 2015, v. 41, No. 5, pp. 508–513

Electronic and magnetic properties of graphite quantum dots

Hazem Abdelsalam[1,2], T. Espinosa-Ortega[3], and Igor Luk'yanchuk[1]

[1]*University of Picardie, Laboratory of Condensed Matter Physics, Amiens 80039, France*
E-mail: lukyanc@ferroix.net

[2]*Department of Theoretical Physics, National Research Center, Cairo 12622, Egypt*

[3]*Division of Physics and Applied Physics, Nanyang Technological University, Nanyang 637371, Singapore*

Received January 15, 2015, published online March 23, 2015

We study the electronic and magnetic properties of multilayer quantum dots (MQDs) of graphite in the nearest-neighbor approximation of tight-binding model. We calculate the electronic density of states and orbital susceptibility of the system as function of the Fermi level location. We demonstrate that properties of MQD depend strongly on the shape of the system, on the parity of the layer number and on the form of the cluster edge. The special emphasis is given to reveal the new properties with respect to the monolayer graphene quantum dots. The most interesting results are obtained for the triangular MQD with zig-zag edge at near-zero energies. The asymmetrically smeared multipeak feature is observed at Dirac point within the size-quantized energy gap region, where monolayer graphene flakes demonstrate the highly-degenerate zero-energy state. This feature, provided by the edge-localized electronic states results in the splash-wavelet behavior in diamagnetic orbital susceptibility as function of energy.

PACS: **75.75.–c** Magnetic properties of quantum dots;
73.21.La Electron states and collective excitation in quantum dots.

Keywords: multilayer quantum dots, tight-binding model, graphite.

1. Introduction

Rise of graphene certainly revived the interest to the classical graphite systems, presenting a wealth of not yet well understood electronic and magnetic properties. The challenge is related to the complicate semimetallic multibranch energy spectrum in the vicinity of the half-field Fermi level, caused by splitting of the Dirac-cone graphene spectrum by the graphite-forming intercarbon-layer coupling. The point of special interest is the crossover from graphene to graphite through the multilayer structures with few number of layers. It is well known that such systems may exhibit metallic or semiconductor behavior as a function of the number of layers and the stacking process [1–5], characteristic that makes them highly appealing for gated controlled electronic devices.

The magnetic properties of few-layer structure are even more intriguing [6–10]. The orbital magnetism of the odd-layer structures is reminiscent to that for the monolayer grapheme [6]. In particularly, a characteristic for graphene diamagnetic δ-function singularity of susceptibility [11,12] appears at the Dirac point at $E = 0$. For even number of layers the magnetic properties are more similar to those for bilayer graphene [6] and the diamagnetic response has the weaker logarithmic divergency. Such odd/even layer decomposition can give the coexistence of Dirac and normal carriers, observed in the pure graphite [13–15].

Alongside, flake-like graphene quantum dots (GQD) have captured the substantial attention of nanotechnology due to their unique optical and magnetic properties [16–29]. The new element here is the finite-size electron confinement, resulted in opening of the energy gap for the bulk delocalized electronic states in the vicinity of Dirac point [16–18,21,22,25]. This gap, however can be filled by the energy level of novel electronic states, localized in the vicinity of the sample boundary [16–18]. For nanoscopic and even for mesoscopic clusters these edge states can play the decisive role in electronic and magnetic properties of the flakes [18–20,28,29]. The situation can drastically depend on size and shape of the clusters. Even the geometrical structure of the edges (armchair vs zig-zag) plays the important role [16,17,25]. In general two types of edge states, located nearby the Dirac point can be discerned, the zero-energy states (ZES) that are degenerate and located exactly at $E = 0$ and the dispersed edge states (DES) that fill the low-energy spectra domain within the gap and are symmetrically distributed with respect to $E = 0$ [23–26].

In this paper, we consider the electronic and magnetic properties of finite-size multilayer quantum dots (MQD) that should generalize the principal features of GQD in that sense as the described above extended multilayer systems grasp the properties of graphene. In particular we show that the edge state located close to $E = 0$ are again responsible for the principal electronic properties, but the level arrangement inside the gap is more diverse as in GQD. To stress the most prominent aspects we consider the characteristics examples of MQD of hexagonal and of triangular shape having zig-zag edges. For calculations we use the approach of tight-binding (TB) model in the nearest neighbor (nn) approximation. For magnetic properties we are mostly concentrated on the orbital diamagnetic effects. The role of the spin-paramagnetic properties is briefly discussed in the conclusion and will be studied elsewhere.

2. The model

Graphene is formed by a two-dimensional honeycomb lattice of carbon atoms in which the conducting π-band electrons can be described within the TB model as

$$H = \sum_i \varepsilon_i c_i^\dagger c_i + \sum_{\langle ij \rangle} (t_{ij} c_i^\dagger c_j + t_{ji} c_j^\dagger c_i), \qquad (1)$$

where $c_i^\dagger$ and c_i are the creation and annihilation electron operators, t_{ij} are the intersite electron hopping elements and ε_i is the on-site electron energy. The Hamiltonian (1) can be extended for the multilayer systems by taking into account the nn hopping between the adjacent layers. Five interlayer coupling parameters $\gamma_1 \ldots \gamma_5$ were introduced by Slonczewski, Weiss and McClure [11,12] as the hopping parameters for the graphite structure (Fig. 1(a)). Parameter $\gamma_1 \simeq 0.39$ eV represents the coupling between the vertically aligned B_N and A_{N+1} atoms (subscript index means the number of plane, shift $N \to N+1$ permutes A and B), parameter $\gamma_3 \simeq 0.315$ eV describes the coupling between the shifted A_N and B_{N+1} atoms and parameter $\gamma_4 \simeq 0.44$ eV corresponds to the coupling between the A_N and A_{N+1} and between the B_N and B_{N+1} atoms. Another two parameters, γ_2 and γ_5 represent the coupling between the next-nearest neighboring (nnn) layers. Parameter $\gamma_5 \simeq 0.04$ eV connects atoms B_N and B_{N+2} belonging to the same vertical line as atoms connected by parameter γ_1 whereas parameter $\gamma_2 \simeq$ $\simeq -0.02$ eV corresponds to another vertically aligned atoms A_N and A_{N+2}, with no intermediate atom between them. In addition, the on-site electron energies ε_i of A and B atoms in layers of MQD become different and described by the gap parameters $\mu_i\Delta$ where $\mu_i = 0$ for A_N and B_{N+1} atoms, $\mu_i = 1$ for A_{N+1} and B_N atoms and $\Delta = \pm 0.047$ eV [5] alternately.

We use the TB Hamiltonian (1) to study the MQD of triangular and hexagonal shape with zig-zag termination. We assume that graphene layers are arranged in the graphite-type ABA stacking as shown in Fig. 1. The electronic energy levels of MQD, E_n, and corresponding DOS are found from the TB Hamiltonian (1) with interlayer hopping. In current article we consider mostly the nn layer coupling, neglecting the effects of γ_2, γ_5 and Δ. The effect of a c-directed magnetic field is accounted by using the Peierls substitution for the hopping matrix elements t_{ij} between atomic sites $\mathbf{r}_i$ and $\mathbf{r}_j$:

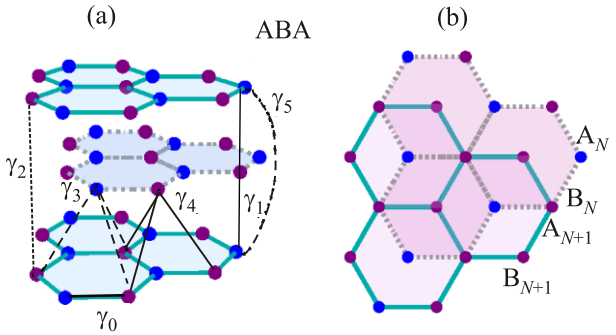

Fig. 1. (Color online) Coupling parameters for multilayer ABA carbon stacking (a). Top view of the multilayer structure (b). The carbon atoms belonging to sublattices A_N and B_N are shown by blue and red colors.

$$t_{ij} \to t_{ij}^P = t_{ij} \exp\left\{ \frac{e}{\hbar c} \int_{\mathbf{r}_i}^{\mathbf{r}_j} \mathbf{A} \cdot d\mathbf{l} \right\}. \qquad (2)$$

Here $\mathbf{A} = (0, Bx, 0)$ is the vector potential of the magnetic field.

Direct numerical diagonalization of Hamiltonian (1) gives the field-dependent energy levels $E_n(B)$ of electronic states and corresponding on-site amplitudes of the wave function $\varphi_{n,i}$. The orbital magnetic energy of the electronic state at $T = 0$ can be found as function of the chemical potential μ and magnetic field B by assumption that all the energy levels below μ are double-filled by spin-up and spin-down electrons:

$$U(B,\mu) = 2 \sum_n^{E_n < \mu} E_n(B). \qquad (3)$$

The corresponding orbital susceptibility per unit area and per one layer is calculated as

$$\chi(\mu) = -\frac{1}{N\sigma} \left[\frac{\partial^2 U(B,\varepsilon)}{\partial B^2} \right]_{B=0}, \qquad (4)$$

where N is the total number of layers and $\sigma = \sqrt{3}a^2 n/4$ is the area of a flake containing n carbon atoms.

3. Graphene quantum dots

Before consider multilayer clusters we describe the principal electronic and magnetic properties of single-layer clusters with zig-zag edges, studied in [16–29].

The DOSs of triangular and hexagonal GQDs with total number of atoms n = 526 and 1014, obtained by diago-

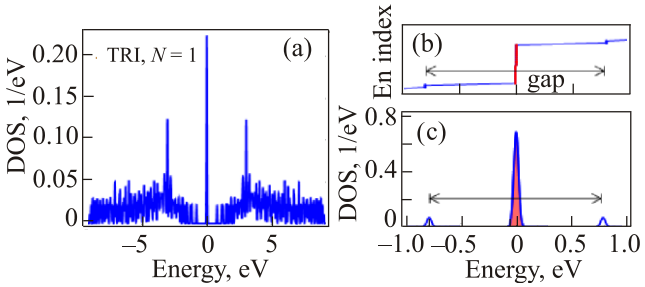

Fig. 2. (Color online) Large-energy scale of DOS of triangular GQD (a), ZES levels (b) and zoom of DOS (c) within the gap region.

nalization of TB Hamiltonian (1) are shown in Figs. 2 and 3. In general, they repeat the DOS of the infinite graphene layer [30] smeared by the finite-quantization noise, that vanishes when size of the cluster increases. The particle-hole symmetry of DOS, $D_1(E) = D_1(-E)$ is conserved.

Figure 4 shows the orbital magnetic susceptibility, obtained from the magnetic field variation of the energy levels by the method, described in Sec. 2. The magnetic field was varied between 0 and 4 T where the susceptibility was checked to be almost field-independent. Again, at large energy scale both the dependencies $\chi(E)$ are similar and are represented by series of jumps between paramagnetic and diamagnetic values, provided by the almost-equiprobable up- and downward displacement of the size-quantized states as function of magnetic field. As cluster size increases, the magnetic susceptibility for all nanostructures, disregarding their shape and edge-termination tends to the bulk limit characterized by a diamagnetic δ-function singularity at $E = 0$ [11].

The most important details, distinguishing triangular and hexagonal GQDs are concentrated at nearly-zero energies when orbital susceptibility is diamagnetic.

The DOS of triangular GQDs (Fig. 2) reveals the remarkable feature: a large number of degenerate states is observed exactly at $E = 0$ and is manifested by the huge central peak of zero-energy states located inside the energy

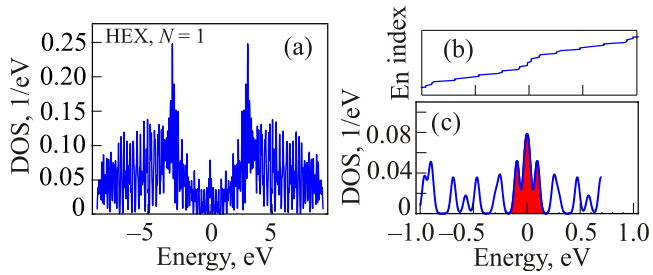

Fig. 3. (Color online) DOS of hexagonal GQD (a), the energy levels (b) and the corresponding DOS in the near-zero-energy region, $E \sim 0$ (c). The levels corresponded to localized edge-states are noted by red color.

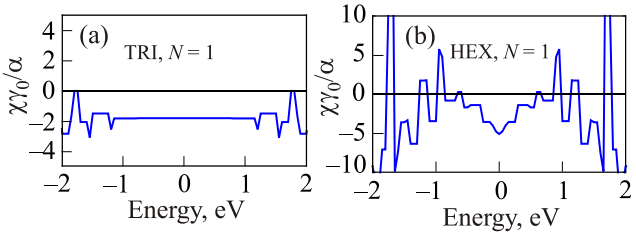

Fig. 4. Orbital magnetic susceptibility of triangular GQD (a) and of hexagonal GQD (b).

gap. This property is explained by the considerable imbalance of atoms in cluster sublattices A and B [18,21] that leads to degeneracy

$$\eta_1 = \sqrt{n+3} - 3. \qquad (5)$$

The wave functions of ZES are localized mainly at the edges of the flake [26].

Absence of electronic states inside the near-zero energy gap results in the field-independent diamagnetic plato in $\chi(E)$ at $E \sim 0$ (Fig. 4(a)). Importantly, the degenerate states from the central peak do not contribute to susceptibility since, they don't move from their location at $E = 0$ when magnetic field is applied.

The level distribution at $E = 0$ in hexagonal GQDs is qualitatively different (see Fig. 3). The localized edge states are not gathered exactly at $E = 0$, but are mostly distributed nearby, inside the band, corresponded to the gap for triangular clusters. In strike contrast to the triangular case, these dispersed states give the considerable contribution to the orbital diamagnetism [26,29], demonstrating the broad diamagnetic peak at $E \sim 0$ in the orbital diamagnetic susceptibility (Fig. 4(b)). In general, the diamagnetic response is larger in hexagonal GQDs as compare to triangular GQDs.

4. Electronic properties of multilayer quantum dots

We turn now to multilayer clusters with layer number $N = 2$–5. The DOSs of triangular MQDs with zig-zag edges are shown in Fig. 5. Similar to the single-layer case the energy gap with the interior central peak in DOS is observed. The difference however is that, these states are not located exactly at the Dirac point $E = 0$ but smeared around it with formation of N peaks of approximately the same amplitude (Fig. 5(b)). The total number of the near-zero energy states (NZES) is just the multiple of ZES in each graphene layer, $\eta_N = N\eta_1$.

To reveal the detailed structure of NZES we plot the eigenstate index vs its energy for different N (Fig. 6) and do observe the energy eigenlevel cumulation at the locations of the split peaks. Importantly, they are not completely degenerate except the states appeared in the odd-layer clusters exactly at $E = 0$. Another new property is the electron–hole asymmetry of DOS with respect to the Dirac

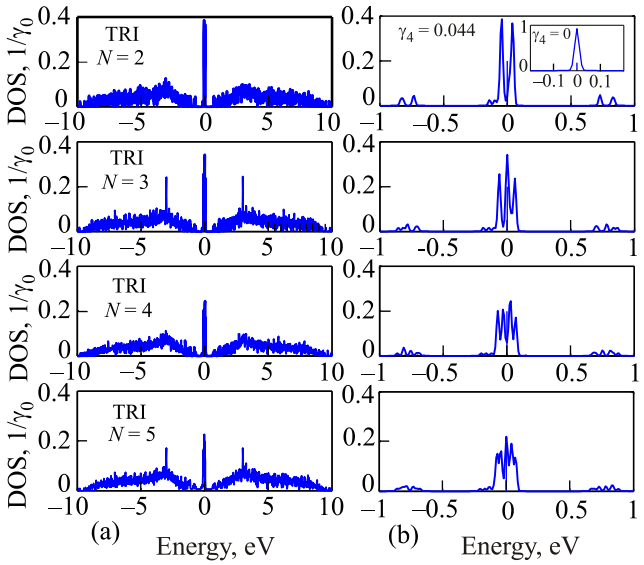

Fig. 5. DOS of triangular MQD with N = 2–5 layers (a) and its zoom at the near-zero energies (b). The nn coupling parameters are indicated in the text. The inset shows the unsplit central peak at $\gamma_4 = 0$.

point, $D_N(E) \neq D_N(-E)$. To examine the origin of these new features we tested the variation of DOS under consecutive variation of the coupling parameters γ_i and found that this is the coupling γ_4 which is responsible for both effects. Inset to Fig. 5(b) shows that the central peak is unsplit at $\gamma_4 = 0$.

Note that $D_N(E)$ for MQDs with $N > 2$ can be reconstructed from DOSs of bilayer clusters of the same shape if the dependence of $D_2(E)$ is known as function of the coupling parameters γ_1, γ_3 and γ_4. Generalizing the band

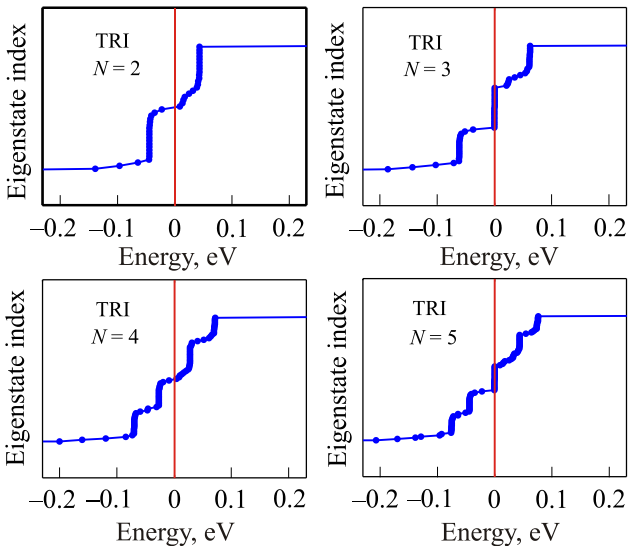

Fig. 6. Energy levels for triangular MQD with N = 2–5 layers inside the gap region.

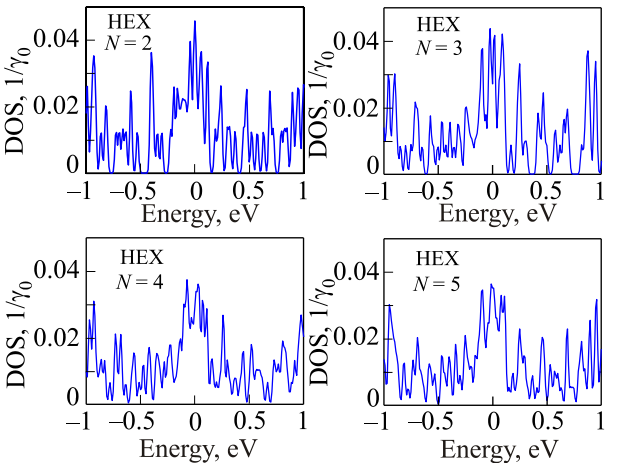

Fig. 7. DOS of hexagonal MQD with N = 2–5 layers in the near-zero-energy region.

decomposition method, proposed for infinite systems in [6] we present $D_N(E)$ as

$$D_N(E) = \frac{1}{2}\sum_m D_2(E, \lambda_{N,m}\gamma_{1,3,4}), \qquad (6)$$

with $m = -(N-1), (N-2), \ldots, N+1$ and with γ-renormalizing scaling factors

$$\lambda_{N,m} = 2\sin\frac{|m|\pi}{2(N+1)}. \qquad (7)$$

Importantly, the term with $m = 0$ and $\lambda_{N,0} = 0$ exists only for the odd number of layers. It corresponds to the contribution from the uncoupled graphene layer, that provides the degenerate ZES observed in Fig. 6. This residual degeneracy however is removed when the nnn couplings γ_2 and γ_5 are taken into account. For even number of layers only two-layers states contribute to $D_N(E)$ and no peaks in DOS appear within the size-quantization gap that vanishes with increasing of the cluster size [31].

Hexagonal MQDs, in contrast to triangular MQDs demonstrate practically the same structure of DOS as the single-layer GQD with near-zero-energy dispersed electronic states (Fig. 7). The only tiny difference is the electron–hole asymmetry, provided by the nn coupling parameter γ_4.

5. Magnetic properties of multilayer quantum dots

The large-energy scale plot of magnetic susceptibility for triangular MQDs with N = 2–5 demonstrates the random oscillations between diamagnetic and paramagnetic states (Fig. 8), similarly to what was observed for the single-layer case. Typically, the absolute values of susceptibility for the odd-layer MQD are always higher than those

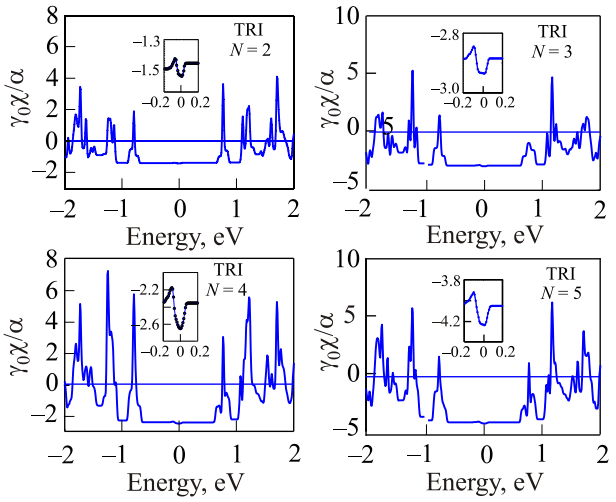

Fig. 8. Susceptibility of triangular MQD with N = 2–5 layers. Insets show the zoom of asymmetric splash-wavelet feature in the near-zero-energy region.

for the even-layer MQDs that can be explained by contribution of one decoupled single-layer, whose susceptibility is remarkably higher [6]. However at $E \sim 0$ the prominent asymmetric splash is revealed in the gap region, where for the $N = 1$ case only the flat energy-independent plato was observed (Fig. 4(a)). This feature is provided by the field-dependent splitting of the central peak due γ_4-coupling.

The structure of $\chi(E)$ for hexagonal MQD (Fig. 9) is approximately the same as for hexagonal GQD, albeit some asymmetry of the broad diamagnetic peak at $E \sim 0$ appears.

6. Discussion

In this paper we studied the electronic and magnetic properties of MQD with zig-zag edges in nn TB approximation as function of the Fermi energy and their relation with similar properties of GQD. The behavior of electronic DOS and of orbital magnetic susceptibility in the near-zero-energy region in vicinity of Dirac point is found to be provided by the edge-localized electronic states. The details substantially depend on shape of MQD and on parity of layer number. In hexagonal MQD the situation is practically the same as in GQD, previously studied in [26]: the quasi-continuum distribution of edge-localized levels is observed at $E \sim 0$ that provides the broad diamagnetic peak in the orbital susceptibility. In contrast, in triangular MQD the qualitatively new feature appears. The highly-degenerate ZES states, centered in the near-zero-energy gap region of triangular GQD, are split by the interlayer coupling parameter γ_4 onto the narrow multipeak band. This gives the nontypical splash-wavelet feature in the orbital diamagnetic susceptibility at Dirac point, absent for GQD.

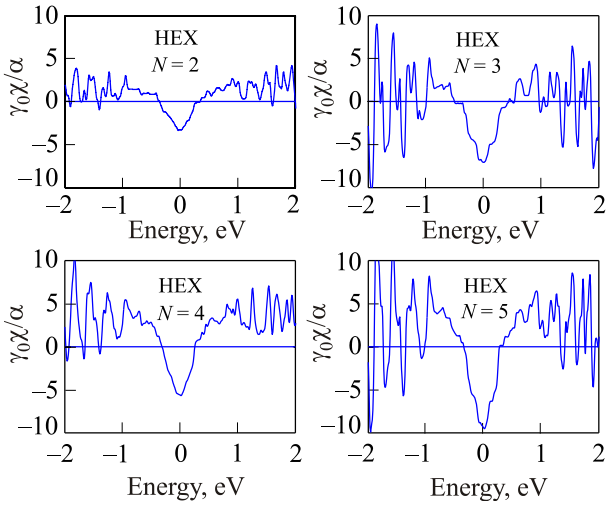

Fig. 9. Susceptibility of hexagonal MQD with N = 2–5 layers.

In our work we were focused on susceptibility arising from the orbital electronic properties whereas the spin-paramagnetic effects were not taken into account. Meanwhile their role can be decisive in case of highly-degenerate electronic states at $E = 0$ in the half-field triangular GQD with zig-zag edges. The smearing of ZES into near-zero-energy band in MQD removes such degeneracy and one can assume that the spin-paramagnetic effects will be less pronounced there. Meanwhile, this question is less trivial when the Hubbard-U Coulomb interaction and temperature-induced intraband electron jumps are properly taken into account. Therefore study of the competition between the temperature-independent orbital-diamagnetic and temperature-dependent spin-paramagnetic properties in MQD posses the challenging problem for many-body statistical physics. These effects can be discerned experimentally, basing on the temperature dependence of susceptibility.

Another interesting property that we observed is the electron–hole asymmetry with respect to the level with E = 0, provided by the same interlayer coupling parameter γ_4. Being of the same origin as asymmetric semimetallic multibranch spectrum of electron–hole carriers in graphite this feature can result in the non-zero location of Fermi level in the half-field MQD. Oscillation of finite DOS at Fermi level as function of magnetic field can give the quasi-de Haas–van Alphen oscillations similar to those observed in the bulk graphite. Study of their character and comparison with graphite presents another challenging problem.

This work was supported by the Egyptian mission sector and by the European mobility FP7 Marie Curie programs IRSES-SIMTECH and ITN-NOTEDEV.

1. S. Latil and L. Henrard, *Phys. Rev. Lett*. **97**, 036803 (2006).
2. B. Partoens and F.M. Peeters, *Phys. Rev. B* **75**, 193402 (2007).
3. J.M.B. Lopes dos Santos, N.M.R. Peres, and A.H. Castro Neto, *Phys. Rev. Lett*. **99**, 256802 (2007).

4. D. Finkenstadt, G. Pennington, and M.J. Mehl, *Phys. Rev. B* **76**, 121405(R) (2008).
5. M. Koshino, *New J. Phys*. **15**, 015010 (2013).
6. M. Koshino and T. Ando, *Phys. Rev. B* **76**, 085425 (2007).
7. S. A. Safran, *Phys. Rev. B* **30**, 421 (1984).
8. R. Saito and H. Kamimura, *Phys. Rev. B* **33**, 7218 (1986).
9. M. Nakamura and L. Hirasawa, *Phys. Rev. B* **77**, 045429 (2008).
10. A.H. Castro Neto, F. Guinea, N.M. Peres, K.S. Novoselov, and A.K. Geim, *Rev. Mod. Phys*. **81**, 109 (2009).
11. J.W. McClure, *Phys. Rev*. **119**, 606 (1960).
12. J.C. Slonczewski and P.R. Weiss, *Phys. Rev*. **109**, 272 (1958).
13. I. Luk'yanchuk and Y. Kopelevich, *Phys. Rev. Lett*. **93**, 166402 (2004)
14. I. Luk'yanchuk and Y. Kopelevich, *Phys. Rev. Lett*. **97**, 256801 (2006)
15. I. Luk'yanchuk, Y. Kopelevich, and M. El Marssi, *Physica B: Condens. Matter* **404**, 404 (2009).
16. M. Ezawa, *Phys. Rev. B* **76**, 245415 (2007).
17. Z.Z. Zhang, K. Chang, and F.M. Peeters, *Phys. Rev. B* **77**, 235411 (2008).
18. J. Fernandez-Rossier and J.J. Palacios, *Phys. Rev. Lett.* **99**, 177204 (2007).
19. W.L. Wang, S. Meng, and E. Kaxiras, *Nano Lett*. **8**, 241 (2008).
20. W.L. Wang, O.V. Yazyev, S. Meng, and E. Kaxiras, *Phys. Rev. Lett*. **102**, 157201 (2009).
21. P. Potasz, A.D. Guclu, and P. Hawrylak, *Phys. Rev. B* **81**, 033403(2010).
22. D.P. Kosimov, A.A. Dzhurakhalov, and F.M. Peeters, *Phys. Rev. B* **81**, 195414 (2010).
23. T. Espinosa-Ortega, I.A. Luk'yanchuk, and Y.G. Rubo, *Superlatt. Microstruct*. **49**, 283 (2011).
24. M. Zarenia, A. Chaves, G.A. Farias, and F.M. Peeters, *Phys. Rev. B* **84**, 245403 (2011).
25. H.P. Heiskanen, M. Manninen, and J. Akola, *New J. Phys*. **10**, 103015 (2008).
26. T. Espinosa-Ortega, I.A. Luk'yanchuk, and Y.G. Rubo, *Phys. Rev. B* **87**, 205434 (2013).
27. J. Liu, Z. Ma, A.R. Wright, and C. Zhang, *J. Appl. Phys*. **103**, 103711 (2008).
28. Y. Ominato and M. Koshino, *Phys. Rev. B* **85**, 165454 (2012).
29. Y. Ominato and M. Koshino, *Phys. Rev. B* **87**, 115433 (2013).
30. J.P. Hobson and W.A. Nierenberg, *Phys. Rev*. **89**, 662 (1953).
31. D.R. da Costa, M. Zarenia, Andrey Chaves, G.A. Farias, and F.M. Peters, *Carbon* **78**, 392 (2014).